Prestrained biaxial DMA investigation of viscoelastic nonlinearities in highly filled elastomers

Dimitri Jalocha, Andrei Constantinescu, Robert Nevière

Prestrained biaxial DMA investigation of viscoelastic nonlinearities in highly filled elastomers

D. Jalocha [a, b, *], A. Constantinescu [a], R. Nevière [b]

[a] *Laboratoire de Mécanique des Solides, CNRS UMR 7649, Ecole Polytechnique, 91128 Palaiseau, France*
[b] *Herakles, Centre de Recherche du Bouchet, 9 rue Lavoisier, 91710 Vert Le Petit, France*

Highly filled elastomers present strong nonlinear mechanical behavior. This study pro-poses a biaxial dynamic mechanical analysis (DMA) experiment to study the prestrain induced nonlinearity. This phenomenon has already been observed for uniaxial tests, revealing an increase of the amplitude of the dynamic modulus with prestrain. The novelty proposed here is to investigate the problem under biaxial conditions. For this purpose, a specific apparatus and an appropriate specimen have been designed. Strains and stresses have been measured using localization formulae and compared with measurements from digital image correlation and finite element computations. Biaxial DMA tests were per-formed on a propellant specimen, for different values of biaxial prestrain. The material is a highly filled elastomer with an important influence of the prestrain on the global visco-elastic behavior. The results exhibit increasing amplitude of the complex modulus with increasing prestrain, as in uniaxial experiments. Moreover, the dependence can be char-acterized using the second invariant of the prestrain, and the viscoelastic behavior is modeled using a closed-form spectrum of relaxation times.

1. Introduction

The combined stiffness and damping behavior of filled elastomers are at the origin of their spread in various application areas. Therefore, they have received high interest as a research subject both in terms of experiments and modeling. Several models have been proposed to describe the nonlinear behavior of reinforced elastomers under large or small strains, monotonic or cyclic loading. There are the models constructed using homogenization theory and applied, for example, to propellants as discussed in [1]. Other models will be phenomenological taking into account damage to be finally compared with experimental observations, as in [2]. In [3] or [4], hyper viscoelastic models are considered under monotonic large strain loading and optimal numerical integration schemes are discussed in detail. Under a cyclic loading regime, one can often observe that viscoelastic behavior of filled elastomers depends on the amplitude of the load during Dynamical Mechanical Analysis (DMA) tests, a phenomenon also known as the Payne effect and discussed, for example, in [5] or [6]. This effect is a consequence of the interactions between fillers and the matrix. An experimental study of the influence of the viscoelastic compressive stress state of the matrix inside filled rubber is reported in [7] and [8]. Recently, an experimental exploration of the outcome of a uniaxial and biaxial prestrain on the viscoelastic properties of highly filled elastomers has been proposed (see [9] and [10]).

The result of the study showed a logarithmic increase of the complex modulus with considerable stiffening once the prestrain exceeds approximatively 1%. In [9], uniaxial

* Corresponding author. Laboratoire de Mécanique des Solides, CNRS UMR 7649, Ecole Polytechnique, 91128 Palaiseau, France.
E-mail address: jalocha@lms.polytechnique.fr (D. Jalocha).

experiments have been described using a simple phenomenological model. The model was able to represent the measured logarithmic evolution of the complex modulus using a generalized Maxwell model. Using an adaptive method, viscous elements were added to the model with increasing prestrain and were able to reproduce the increasing stiffness. Later, in [10] a biaxial prestrained DMA experiment was proposed where one of the axial directions of the cruciform specimen was blocked at a given prestrain level, and DMA tests were performed in the orthogonal direction. In this paper, we present biaxial DMA experiments superimposed on a fully biaxial prestrain. Moreover, we show that a viscoelastic model constructed using the continuous spectrum of relaxation times accurately describes the experimental results.

The material under scrutiny is a propellant. These materials are classified as being in the family of highly filled elastomers and are used for solid propulsion of rockets and launchers. Propellants are constituted, up to 70% of their volume, by fillers bonded together by a viscoelastic matrix [11]. Their functioning during the oxidation-reduction reaction of the fillers releases pressurized gases inside a confined chamber which are then ejected through a nozzle and propel the structure [12]. The energetic properties of the propellant guarantee the efficiency of the engine, whereas the mechanical properties govern structural performances such as stability and integrity. In spite of the small volume fraction of the polymeric matrix, its intrinsic behavior will induce viscoelastic behavior of the composite solid propellant. Moreover, the high volume fraction of fillers will induce strong nonlinearities [13]. Recently, a complete characterization of the uniaxial prestrain influence has been performed for a solid propellant in [14]. The nonlinear viscoelastic model has been represented by the spectrum of relaxation times of the material and the properties have been assessed using both relaxation and DMA experiments.

The aim of this paper is to revisit the topic of prestrain induced nonlinearities on the viscoelastic properties during DMA tests. The prior results are extended both in term of experimental complexity and modeling. On the one hand, the experiment discussed here imposes a prestrain and applies biaxial cyclic loads on both directions of the specimen; on the other hand, the results are interpreted using a model of the relaxation spectrum of the viscoelastic material depending on the applied prestrain level. The proposed model can then be transformed into a Generalized Maxwell model and the associated Prony series. However, this expansion will not be presented here.

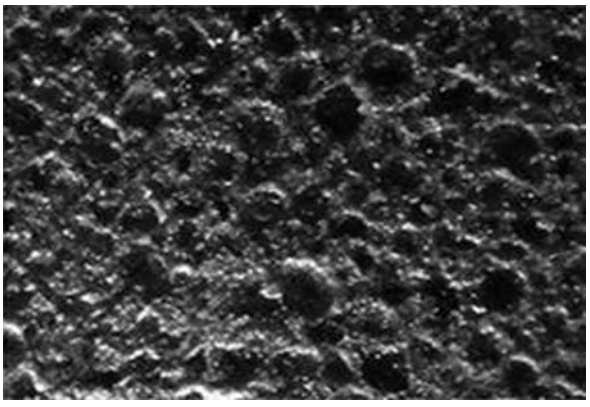

Fig. 1. Micrography of solid propellant, fillers (in black) bonded by the matrix (in gray).

This paper starts with a description of the material and is followed by a review of a suitable uniaxial prestrain dependent model of the relaxation spectrum represented by a closed-form expression. Next, the biaxial test machine and the measurement method are presented. Finally, the results of the biaxial DMA with prestrain are discussed and compared with preceding results from uniaxial measurements. The analysis is based on the closed-form expression of the relaxation spectrum.

2. Material

The material used here is propellant, a highly filled elastomer with complex nonlinear behavior. The nonlinearity is due to the extremely high filler fraction and the consequence of an extremely thin binder region between the filler particles. More precisely, the propellant consists of a cross-linked elastomeric matrix based on hydroxy-terminated polybutadiene (HTPB) in which the fillers composed of ammonium perchlorate and aluminum particles are included (see Fig. 1 and described in detail, for example, in [15]). The mechanical properties of the composite will inherit the viscoelasticity of the matrix and stiffness of the inclusions. Fillers constitute up to 70−80% of the volume, placing propellants at the higher end of highly filled elastomers, far beyond rubber where carbon black fillers will only add up to 30−50% of the volume (in tires for example). Moreover, due to the high volume fraction of the fillers, the manufacturing process will induce an over reticulated HTPB matrix. Two phases can be distinguished in the polymeric matrix: a principal cross-linked network connecting and fastening the fillers, and free polymer chains floating inside the network, which are neither linked to the filler nor to the principal network. A detailed analysis of the physical bases of this assumption is given and already discussed in [16], [17]. A schematic representation of the explanation is displayed in Fig. 2. The physical and mechanical interactions between the fillers and the binder or between the phases of the polymeric matrix are at the origin of the observed mechanical nonlinearities at the scale of the composite. These relations between the physical interactions and the macroscopic properties as a function of different input parameters have been extensively discussed in [15].

3. Model

The aim of the paper is analyze the viscoelastic material behavior. Moreover, we consider for the sake of simplicity, without restraining the generality of the approach, the deformation of material only in the small strain range and under the constraint of incompressibility.

Viscoelasticity can be expressed in the time or the frequency domain, as classically explained, for example, in the

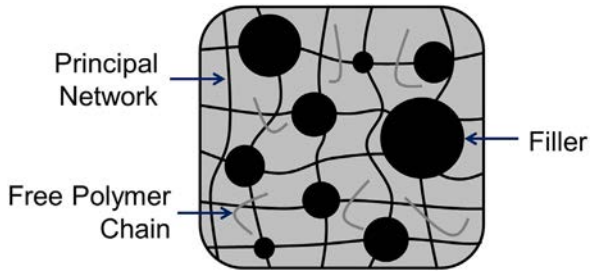

Fig. 2. Schematic representation of solid propellant.

textbook [18]. In the time domain, viscoelasticity is described by the time dependent relaxation modulus $E(t)$, which is directly measured during a relaxation test [19]. In the frequency domain, the viscoelasticity is described by the frequency dependent dynamic modulus $E^*(\omega)$, measured during a DMA test [20]. The relaxation and the dynamic moduli are related to a unique relaxation time spectrum H(τ) depending on the time τ. The spectrum H completely characterizes the viscoelastic material behavior [21]. For polymers, consisting of long molecular chains, this spectrum can be interpreted as the statistical distribution of the molecular mobility of the polymer chains [22]. Several algorithms have been proposed in the literature to identify the relaxation function H, either from the measured relaxation modulus as in [23], or from the measured components of the complex dynamic modulus as in [24].

The constitutive law is written in the frequency domain as:

$$\sigma^*(\omega) = E^*(\omega)\varepsilon^*(\omega) \tag{1}$$

where $\sigma^*(\omega)$ and $\varepsilon^*(\omega)$ denote the Fourier transform of the stresses and strains as a function of frequency ω, respectively. Moreover, by definition, the complex modulus is expressed as a function of the relaxation time spectrum H(τ):

$$E^*(\omega) = \int_{-\infty}^{+\infty} H(\tau)\frac{i\omega\tau}{1+i\omega\tau}d\ln(\tau) \tag{2}$$

In a recent study [14], the spectrum for solid propellant was identified from both time domain and frequency domain results. The following additive representation of the relaxation spectrum H(τ) has been proposed:

$$\begin{aligned} H(\tau) &= \frac{E_{g1}}{\Gamma(\beta_1)}\left(\frac{\tau}{t_1}\right)^{-\beta_1} e^{-\frac{t_1}{\tau}} + \frac{E_{g2}}{\Gamma(\beta_2)}\left(\frac{\tau}{t_2}\right)^{-\beta_2} e^{-\frac{t_2}{\tau}} \\ &\quad + \frac{E_{g3}}{\Gamma(\beta_3)}\left(\frac{\tau}{t_3}\right)^{-\beta_3} e^{-\frac{t_3}{\tau}} \\ &= H_1(\tau) + H_2(\tau) + H_3(\tau) \end{aligned} \tag{3}$$

where $(E_{gi}, \beta_i, ti)_{i=1,3}$ are adjustable parameters and Γ is the Euler Gamma function. More precisely, the spectrum is the sum of three terms. Each term corresponds to a specific component of the polymeric network representing the binder. The evolution of the spectrum H and of its three components as a function of time τ is represented in Fig. 3. The first term, denoted with the subscript "1", is the viscoelastic relaxation signature of the molecular mobility of the principal network. The second term, denoted with the subscript "2", is the signature of the molecular mobility of the unlinked polymer chains. The third term, denoted by subscript "3", represents the signature of the long time molecular mobility of polymer. This additive decomposition, as well as the relations with the phases of the polymer network, is coherent with the previous observations and measurements done in [16]. One can observe that the first two families have significant importance on the distribution of H, whereas the last one is visible only when compared to the values at long times.

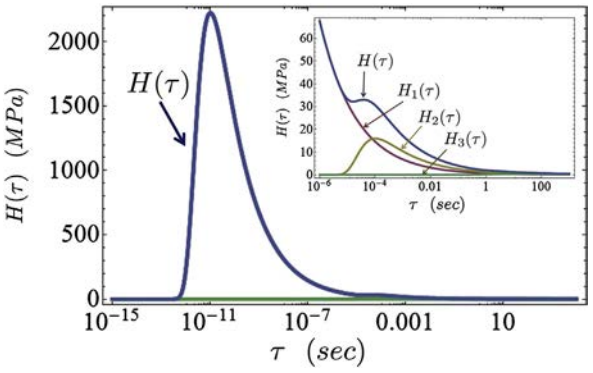

Fig. 3. Relaxation time spectrum of solid propellant $H(\tau)$, identified in [14]. The smaller panel described the contributions of the three terms. The second contribution $H_2(\tau)$ contains prestrain dependent exponent.

As discussed in previous work [14], a series of uniaxial prestrained DMA experiments were used to identify the parameters of the preceding model (3). More precisely, it has been shown that we can correlate the influence of the prestrain with a variation of exponent β_2. The exponent characterizes the signature of the molecular mobility of the unlinked polymer chains. This chain will float between islands of the polymer network and the fillers. When a prestrain is applied, fillers will close up and the unlinked polymer chains will be restricted in their movement. The relation between β_2 and the axial prestrain ε_{s1} (see Fig. 9)

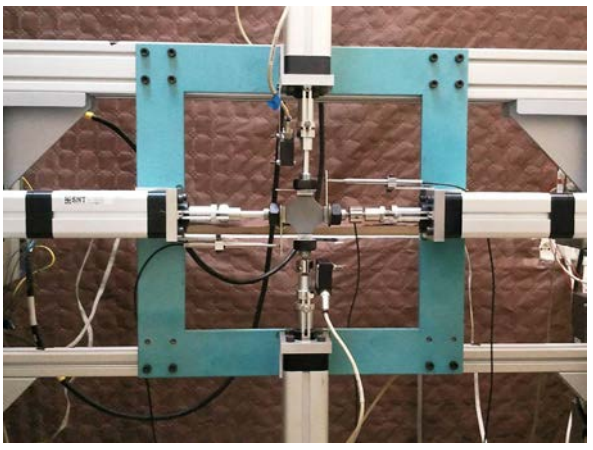

Fig. 4. Biaxial apparatus used for biaxial prestrain DMA experiments with the cruciform shape specimen in the center.

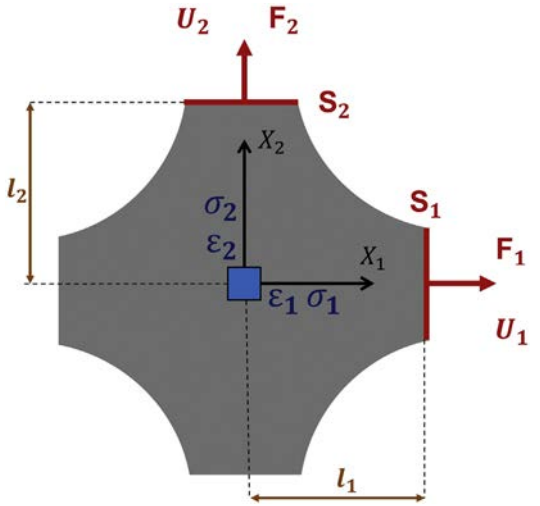

Fig. 5. Schematic representation of the specimen. (U_i, S_i, F_i) are the displacement, surface and force at the end of the arms of the specimen. $\underline{\underline{\varepsilon}}$ and $\underline{\underline{\sigma}}$ are the strain and stress in the central area of the specimen.

obtained as a result of the uniaxial prestrained DMA experiment is displayed in Fig. 12.

One can further remark that the model proposed here is different from the model developed in [9] or [10] where elements are added step by step in a Generalized Maxwell model, as a function of the increasing prestrain. The model here is described by the continuous spectrum H(τ) with only one prestrain dependent parameter, and is not directly related to a Generalized Maxwell model [25]. However, the relaxation spectrum presented previously can be discretized a posteriori into a Generalized Maxwell Model and described by a Prony series [26].

The next objective is to explore the influence of an orthogonal prestrain ε_{s2} superimposed on an axial prestrain ε_{s1} on the viscoelastic properties as represented by E^*.

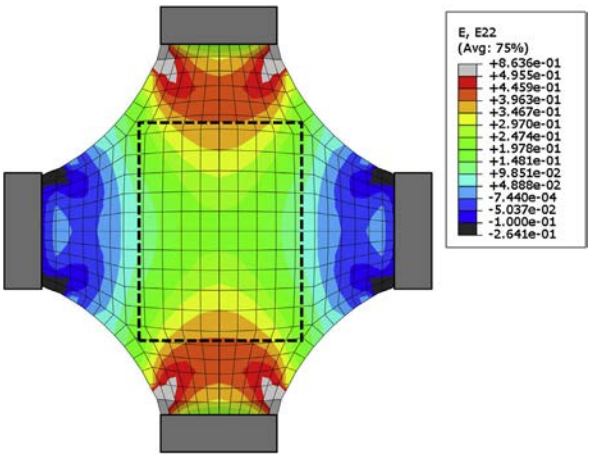

Fig. 6. Elastic Finite Element Analysis of the specimen driving to the computation of the microscopic strain and stress in the center of the specimen from the macroscopic strain and stress of each termination.

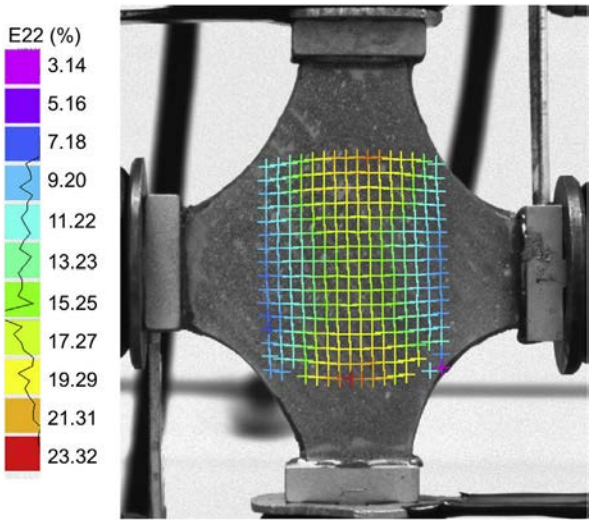

Fig. 7. Digital Image Correlation performed on the specimen during a biaxial experiment. It permits to compare the measured microscopic strain with the computed microscopic strain using the transfer function.

4. Biaxial experimental setup

The biaxial DMA tests under biaxial prestrain have been performed using a biaxial tensile testing setup. The machine was constructed from independent parts following the design proposed in [27] or [28]. The set-up consists of four electric actuators fixed on a rigid rectangular frame. The actuators will finally form a cross on the frame. The biaxial machine is pictured in Fig. 4. The actuators are high precision electric motors NTM-207 with a linear movement transformer ISOMOVE 50 manufactured by SNT [29]. The displacements of the four actuators are measured by four

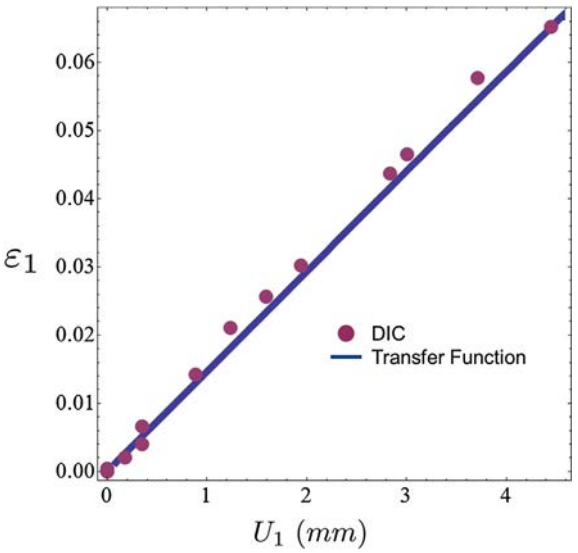

Fig. 8. Comparison between strain computed by the transfer function and strain measured by DIC in the center of the specimen in function of the macroscopic displacement U_1 and $U_2 = 0$.

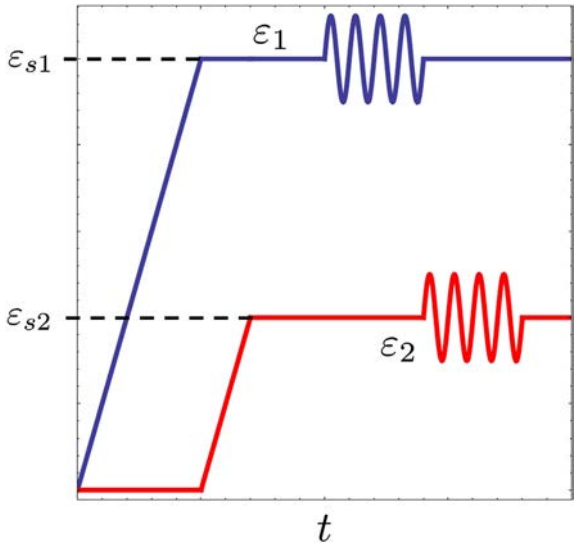

Fig. 9. Evolution of the imposed strain in the X_1 and X_2 direction as a function of time. A first prestrain is imposed in the X_1 direction followed by the prestrain in the direction X_2. Finally a sinusoidal strain is superimposed prestrain in both the X_1 and the X_2 direction to measure the dynamic modulus.

WA-T Linear Variable Differential Transformer sensors provided by HBM [30]. The maximal measured displacement range is 30 mm. The force acting in each axis is measured by a force transducer U9B manufactured by HBM [30]. Finally, the loading and measurement range of the applied force lies between 0 and 1kN.

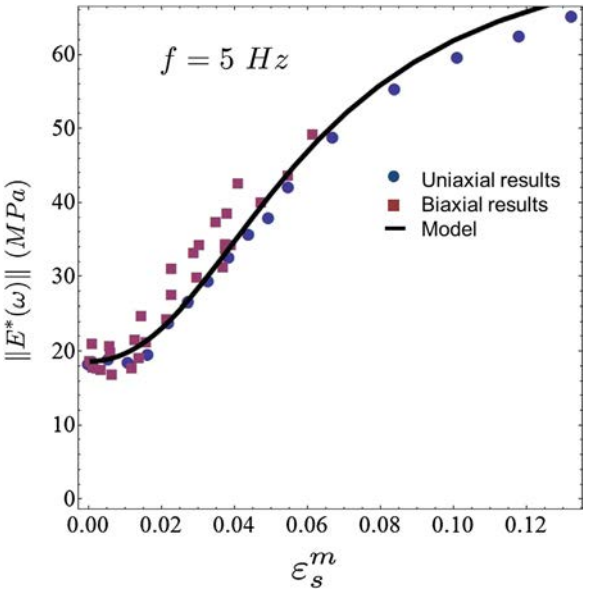

Fig. 10. Amplitude of the dynamic modulus as a function of the second invariant of the prestrain at frequency of 5 Hz, measured in uniaxial (blue circles) ([14]) and biaxial (violet square) experiments and compared with predictions from model. (For interpretation of the references to color in this figure legend, the reader is referred to the web version of this article.)

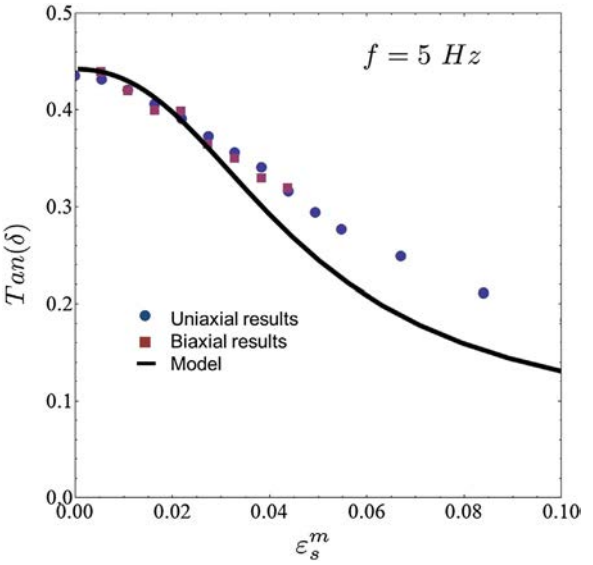

Fig. 11. Phase angle evolution in function of the second invariant of the prestrain for a frequency equal to 5 Hz. Uniaxial (blue circles) ([14]) and biaxial (violet square) results are given. The evolution is the same for the two kind of tests. The model (black solid line) reproduces this evolution, but tends to over estimate the experiments. (For interpretation of the references to color in this figure legend, the reader is referred to the web version of this article.)

An important feature for biaxial testing is the precise shape of the specimen. The optimal specimen should be free of stress or strain singularities and needs a large central area where the material is under biaxial strain. For metallic specimens, this is achieved by creating a thinner circular area in the middle of the specimen, as discussed in [31] for a cruciform specimen. A thinner central zone results in better control of the strain and stress in the center. Taking into account the manufacturing process of the propellant, one cannot create a thinner central area in order to achieve

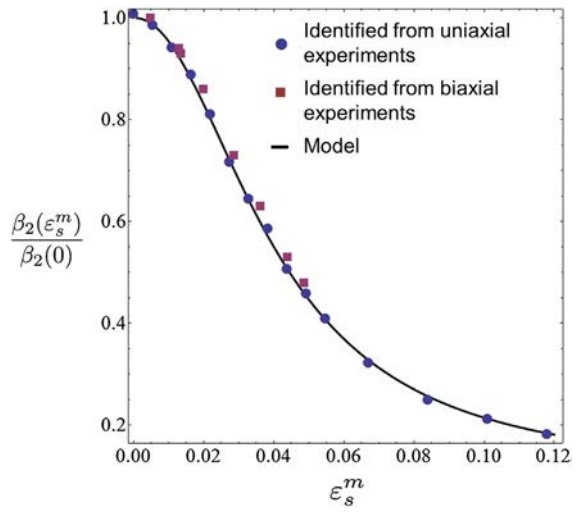

Fig. 12. Evolution of the parameter β_2 as a function of the second invariant of the prestrain.

this goal. As a consequence, alternative solutions are needed to solve the problem. Many authors have looked for a special geometry specimen which optimizes the biaxial strain and stress fields. Specimens with an optimized blending radius are proposed to reduce the stress localizations in [32]. A solution consisting of elongated holes along both axis of the cruciform specimen has been proposed in [33]. This specimen reduces the stress concentration, by keeping a simple specimen geometry.

In the present study, as in [10], the specimen will keep its cruciform shape (see a schematic view displayed in Fig. 5). However, the small radii are replaced by large radius and the effect on the stress and strain distribution has been discussed in [10]. Each end termination of the arms of the cross is glued to a grip, which is finally fixed to the actuator.

The displacements (U_1, U_2) and the forces (F_1, F_2) are directly measured at the end of the arms of the specimen using specific gauges. Knowing the distances (l_1, l_2) and the surfaces (S_1, S_2), the strain $\underline{e} = (e_1, e_2)^T$ and stress $\underline{\Sigma} = (\Sigma_1, \Sigma_2)^T$ can be computed as:

$$\Sigma_i = \frac{F_i}{S_i} \quad e_i = \frac{U_i}{l_i} \quad \left(i = 1,2\right) \tag{4}$$

For the material determination, the objective is to have local information of the biaxial strains $\underline{\underline{\varepsilon}}$ and stresses $\underline{\underline{\sigma}}$ in the central area from the global strain and stresses measured before, without measuring or computing the complete heterogeneous fields over the specimen.

In order to recover the local fields, we follow the approach proposed in [10] which is based on the assumption of a linear relation between global and local fields. Therefore, the relations are reduced to knowledge of two matrixes, denoted as strain and the stress transfer functions (L_ε and L_σ respectively). The relation between measured and computed quantities is given by the expressions:

$$\underline{\underline{\varepsilon}} = \mathbb{L}_\varepsilon \underline{e} \quad \underline{\underline{\sigma}} = \mathbb{L}_\sigma \underline{\Sigma} \tag{5}$$

The transfer functions are determined from finite element solutions, under the assumption of elastic material behavior (see Fig. 6). The transfer functions are computed from strain and stress values in the center of the specimen and the values at the end section by minimizing the least squares distance. The approximation has been validated up to strain of 10%. A subsequent assumption, already verified in [10], is that the transfer function computed with the elastic solution will be equally valid in the viscoelastic domain.

Next, we enhance the prior validation of the transfer functions using the strain field from Digital Image Correlation (DIC). DIC was performed using a CorrelManuV [34] software package (see Fig. 7). The pixel size was 6×6 μm^2 and the image was recorded over an area of 3×3 cm^2. On the left panel, we displayed the results of the finite element computation and on the right panel the measured strain field. One can observe the good match between computations and measurements.

For comparison, Fig. 8 presents the experimental values of the strain ε_1 measured by DIC in the center of the specimen, and the corresponding strain computed using the transfer function for a macroscopic imposed displacement U_1. The displacement in the X_2 direction is blocked ($U_2 = 0$). The match is good and can be characterized by a relative error of $2^{\pm 1}$ %. As a consequence, hereafter, we shall make systematic use of the values of strain and stress computed with the transfer function.

Another result of the finite element computations concerns the tensorial form of strains and stresses in the central zone of the specimen. The computations show that strains and stresses are diagonal and that principal axes are oriented along the directions of the cross, as expected in a biaxial experiment. Moreover, the incompressibility assumption permits computation of the strain in the third direction ε_3. As a final consequence, one can state that the strain and stress transfer functions depend only on the geometry of the specimen.

Recalling that the goal of this work is to measure the dynamic modulus $E^*(\omega)$ under biaxial prestrain, and taking into account the arguments of the preceding discussion, the complete experimental procedure including the imposition of the prestrain will be defined in the next steps:

1. Impose a prestrain ε_{s1} in the X_1 direction.
2. Impose a prestrain ε_{s2} in the X_2 direction.
3. Under the biaxial prestrain state (ε_{s1}, ε_{s2}), superimpose a sinusoidal strain in the X_1 direction taking the form $\varepsilon_1(t) = \varepsilon_{s1} + \varepsilon_d \, sin(\omega t)$ maintaining $\varepsilon_2 = \varepsilon_{s2}$. The sinusoidal stress $\sigma_1(t)$ in the X_1 direction is recorded.
4. Under the biaxial prestrain state (ε_{s1}, ε_{s2}), superimpose a sinusoidal strain now in the X2 direction taking the form $\varepsilon_2(t) = \varepsilon_{s2} + \varepsilon_d \, sin(\omega t)$ maintaining $\varepsilon_1 = \varepsilon_{s1}$. The sinusoidal stress $\sigma_2(t)$ in the X_2 direction is recorded.

A schematic representation of the procedure is displayed in Fig. 9. The experiments were performed for strain amplitude of $\varepsilon_d = 0.4\%$ with a pulsation $\omega = 2\pi f$ at a frequency of $f = 5Hz$.

One can remark that the order and the simultaneity of imposing prestrain or the sinusoidal load does not affect the final result. The order and the simultaneity do not affect the measurement of the dynamic moduli but modify the value of the various strain amplitudes.

The measurement of the viscoelastic properties is performed in two steps: first, strains and stresses are estimated in the center of the specimen and, second, the dynamic modulus $E^*(\omega)$ is computed using the Fourier Transform. Considering two sinusoidal signals ε_i and σ_i (with i = 1,2), the dynamical amplitude of each signal is defined by the maximum of the Fast Fourier transform $\mathscr{F}(\varepsilon_i)$ and $\mathscr{F}(\sigma_i)$, respectively. The phase angle between the signals is set by the maximum of the ratio $\mathscr{F}(\sigma_i)/\mathscr{F}(\varepsilon_i)$. A complete explanation of the Fast Fourier Transforms analysis of two sinusoidal signals is extensively explained, for example, in [35].

An analysis of the algorithm shows that, after the third step, using the signals $\sigma_1(t)$ and $\varepsilon_1(t)$, one can compute the complex modulus E_1^* corresponding to direction X_1. Then, after the forth step, using the signals $\sigma_2(t)$ and $\varepsilon_2(t)$, one can compute the complex modulus E_2^* in the X_2 direction.

Table 1
Identified parameters for the relaxation time spectrum (Equations (3) and (6)) describing the nonlinear viscoelastic behavior of solid propellant (E_{gi} in [MPa], t_i in [s] and β_i, ε_r, q dimensionless).

E_{g1}	t_1	β_1	E_{g2}	t_2	β_2^0	ε_r	q	E_{g3}	t_3	β_3
12191	3×10^{-12}	0.333	91	3×10^{-5}	0.312	0.045	2.1	6	1.27	0.07

The experimental procedure and the data processing described so far provide, for each biaxial prestrain pair (ε_{s1}, ε_{s2}), the dynamic moduli E_1^* and E_2^* corresponding to the two directions.

5. Results and discussion

Let us recall that the studied material is isotropic. Therefore, we expect to recover several symmetries on the measured moduli. For any prestrain state, the dynamic modulus is independent of the direction of the measure: $E_1^*(\varepsilon_{s1}, \varepsilon_{s2}) = E_2^*(\varepsilon_{s1}, \varepsilon_{s2})$. Moreover, the prestrains ε_{s1} and ε_{s2} are symmetrical, therefore the directions X_1 and X_2 can be interchanged and the measure of the dynamic modulus provides the same result: $E_1^*(\varepsilon_{s1}, \varepsilon_{s2}) = E_1^*(\varepsilon_{s2}, \varepsilon_{s1})$. As a consequence, we can consider that the dynamic modulus depends only on the angular frequency ω and on the second invariant of the prestrain defined by: $\varepsilon_s^m = \sqrt{\frac{2}{3}\underline{\underline{\varepsilon_s}} : \underline{\underline{\varepsilon_s}}}$.

The previous assumptions permit now to compare measured values of the complex modulus both from uniaxial results, obtained in [14], and biaxial loadings. The measurements of the amplitude and the phase angle of the dynamic modulus and a model prediction are displayed in Fig. 10 and Fig. 11 as a function of the second invariant of the prestrain. We note that the dynamic modulus and the phase angle in both uniaxial and biaxial experiments follow close evolutions as a function of the second invariant of the prestrain. The spread of the data is larger for the dynamic modulus as it depends essentially on the measured strain, whereas phase angle is related to the time shift in the measured signal. Another source of the spread is small heterogeneity of the mechanical properties of the propellant.

Therefore, the spectrum of relaxation time $H(\tau, \varepsilon_s^m)$ depends now on the time and on the second invariant of the prestrain. The material parameters of the model Equation (3) are identified using the nonlinear solver of Mathematica® (NonLinearModelFit [36]). The model prediction in Figs. 10 and 11 was obtained in following steps. The model presented in Equation (3) is supposed to have a prestrain dependent coefficient β_2. Moreover, we define the following expression:

$$\beta_2(\varepsilon_s^m) = \frac{\beta_2^0}{1 + \left(\frac{\varepsilon_s^m}{\varepsilon_r}\right)^q} \tag{6}$$

Fig. 12 presents the comparison of experimental and predicted values of β_2 as a function of ε_s^m. The experiment values are identified directly from axial and biaxial experiments, and the model is the least square approximation obtained from Equation (6), where β_2^0, ε_r, q have been considered real parameters (see Table 1).

The predictions of the model match the different experimental results. In Fig. 10 and Fig. 11, we note the excellent prediction for the amplitude of the dynamic modulus and a small underestimation of the phase angle. The average relative error is $6^{\pm 3}$ % for the amplitude of the dynamic modulus and $8^{\pm 4}$ % for the phase angle.

Fig. 13 presents the biaxial and uniaxial measurements in terms of the amplitude of the dynamic modulus plotted against the two values of prestrain (ε_{s1}, ε_{s2}). The points are the experimental measurements and surface is obtained by the model, as discussed previously. The height represents the amplitude of the dynamic modulus. We obtain a good match between the model predictions represented by the surface and the biaxial measures displayed as points as in Fig. 10. However, the maximal relative error is around 15%.

6. Conclusions

The viscoelastic material behavior of highly filled elastomers under orthogonal prestrain embodies important nonlinearities. This study presents a method of conducting biaxial DMA experiments with orthogonal prestrain. The prestrain was applied in two orthogonal directions and the DMA experiments were performed in the same directions. This represents a generalization of the setting discussed in [10] but needed the complete design of a biaxial

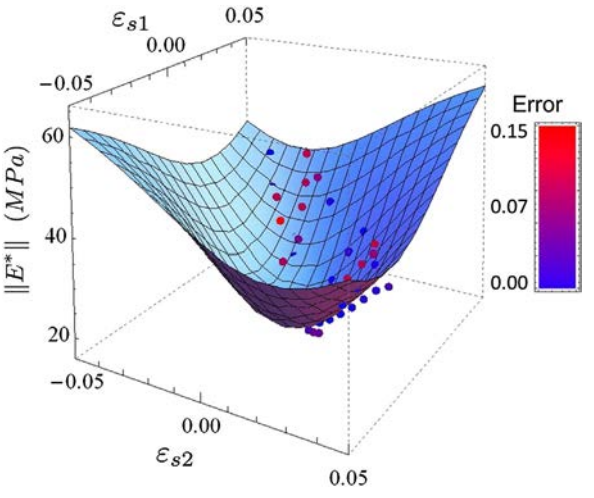

Fig. 13. Comparison between experimental results (points) and model prediction (surface) for the amplitude of the dynamic modulus, as a function of the prestrain. The color of the point is the relative error in the scale display on the right hand side of the plot. (For interpretation of the references to color in this figure legend, the reader is referred to the web version of this article.)

experimental apparatus. The shape of the specimen and the transfer functions used for the fast computation of the stress and strain values in the center of the cross-shaped specimen from measures at the end of the arms were further validated using a comparison of finite element computation with field measurements using digital image correlation.

The viscoelastic material properties expressed as complex elastic modulus as a function of prestrain of a propellant material were characterized using the present experimental apparatus. The results exhibit a dependence of the complex elastic modulus on the second invariant of the prestrain. As a general result, it can be stated that the amplitude of the modulus increases with respect to the second invariant of prestrain, whereas the phase angle decreases.

The material behavior was modeled using a closed-form expression of the relaxation spectrum. One of the parameters in the closed-form expression was modified to express the dependence of the second invariant of prestrain. The complete set of parameters of the relaxation spectrum was identified from both uniaxial and biaxial experimental results. The model predictions were a good match for the experimental results.

This study opens new perspectives in the measurement of the prestrain dependent properties of viscoelastic materials. The new measurements will challenge the theoretical constitutive models to take these results into account in order to represent complete three-dimensional behavior as needed in structural computations.

Acknowledgements

The authors would like to thank the Direction Generale de l'Armement (DGA, France), Laurent Munier (DGA), and SAFRAN HERAKLES for financial support for this study.

References

[1] F. Xu, N. Aravas, P. Sofronis, Constitutive modeling of solid propellant materials with evolving microstructural damage, Journal of the Mechanics and Physics of Solids 56 (2008) 2050–2073.
[2] R.A. Schapery, A micromechanical model for non-linear viscoelastic behavior of particle reinforced rubber with distributed damage, Engineering Fracture Mechanic 25 (1986) 845–853.
[3] J. Simo, On a fully three-dimensional finite-strain viscoelastic damage model: formulation and computational aspects, Computer Methods in Applied Mechanics and Engineering 60 (1987) 153–173.
[4] P. LeTallec, C. Rahier, Numerical models of steady rolling for nonlinear viscoelastic structures in finite deformations, International Journal for Numerical Methods in Engineering 37 (1994) 1159–1186.
[5] A. Payne, The dynamic properties of carbon black-loaded natural rubber vulcanizates. part i, Journal of Applied Polymer Science 6 (1962) 5357–5369.
[6] A. Lion, C. Kardelky, The Payne effect in finite viscoelasticity: constitutive modelling based on fractional derivatives and intrinsic time scales, International Journal of Plasticity 20 (2004) 1313–1345.
[7] G. Ravichandran, C.T. Liu, Modeling constitutive behavior of particulate composites undergoing damage, International Journal of Solids Structure 32 (1995) 979–983.
[8] A. Amin, A. Lion, S. Sekita, Y. Okui, Nonlinear dependence of viscosity in modeling the rate-dependent response of natural and high damping rubbers in compression and shear: experimental identification and numerical verification, International Journal of Plasticity 22 (2006) 1610–1657.
[9] A. Thorin, A. Azoug, A. Constantinescu, Influence of prestrain on mechanical properties of highly-filled elastomers: measurements and modeling, Polymer Testing 31 (2012) 978–986.
[10] A. Azoug, A. Thorin, Robet Neviere, Rachel-Marie Pradeilles-Duval, Andrei Constantinescu, Influence of orthogonal prestrain on the viscoelastic behavior of highly-filled elastomers, Polymer Testing 32 (2013) 375–384.
[11] S. Ozupek, Constitutive Modeling of High Elongation Solid Propellants, PhD thesis, University of Texas, 1989.
[12] A. Azoug, Micromecanismes et comportement macroscopique d'un elastomere fortement chargement, PhD thesis, Ecole Polytechnique, 2010.
[13] S. Ozupek, E. Becker, Constitutive modeling of high-elongation solid propellants, Journal of Engineering Material and Technology-Trans. ASME 114 (1992) 111–115.
[14] D. Jalocha, A. Constantinescu, R. Niviere, Prestrain dependent viscosity of highly filled elastomer: experiments and model, Mechanics of Time Dependent Material (2015). Submitted for publication.
[15] A. Azoug, A. Constantinescu, R. Pradeilles-Duval, M.F. Vallat, R. Neviere, B. Haidar, Effect of the sol fraction and hydrostatic deformation on the viscoelastic behavior of prestrained highly filled elastomers, Journal of Applied Polymer Science 127 (2013) 1772–1780.
[16] A. Azoug, A. Constantinescu, R.M. Paridelles Duval, R. Neviere, Influence of cross-linking and plasticizing on the viscoelasticity of highly-filled elastomers, Journal of Applied Polymer Science 131 (2014) 201–215.
[17] A. Azoug, A. Constantinescu, R.M. Paridelles Duval, R. Neviere, Influence of fillers and bonding agents on the viscoelasticity of highly-filled elastomers, Journal of Applied Polymer Science 131 (2014) 321–325.
[18] H. Brinson, Polymer Engineering Science and Viscoelasticity. An Introduction, 2008.
[19] W. Findley, J. Lai, K. Onaran, Creep and Relaxation of Nonlinear Viscoelastic Materials, 1976.
[20] W. Knauss, L. Emri, H. Lu, Handbook of Experimental Solid Mechanics, Spinger, 2006.
[21] M. Baumgaertel, H. Winter, Interrelation between continuous and discrete relaxation time spectra, Journal of Non-Newtonian Fluid Mechanics 44 (1992) 15–36.
[22] P. de Gennes, Scaling Concept in Polymer Physics, Cornell University Press, Ithaca, New York, 1979.
[23] S. Bhattacharjee, A. Swamy, J. Daniel, Continuous relaxation and retardation spectrum method for viscoelastic characterization of asphalt concrete, Mechanics of Time Dependent Materials 16 (2012) 287–305.
[24] V. Shtrauss, A. Kalpinsh, Determination of relaxation and retardation spectrum from modulus of complex frequency domain material functions, Transactions on Applied and Theoretical Mechanics 7 (2012) 29–35.
[25] Simo, Hughes, Wiggins, J. M. L. S. S. Computational Inelasticity, in: Interdisciplinary Applied Mathematics, 1998.
[26] T. Smith, Empirical equations for representing viscoelastic functions and for deriving spectra, Journal of Polymer Science 35 (1971) 39–50.
[27] A new biaxial tension test fixture for uniaxial testing machine: a validation for hyper elastic behavior of rubber-like materials, Journal of Testing and Evaluation 35 (2007) 35–44.
[28] M. Johlitz, S. Diebels, Characterisation of a polymer using biaxial tension tests, Archive of Applied Mechanics 81 (2011) 1333–1349.
[29] http://www.snt.tm.fr/.
[30] http://www.hbm.com/fr/.
[32] N. Bhatnagar, R. Bhardwaj, P. Selvakumar, M. Brieu, Development of a biaxial tensile test fixture for reinforced thermoplastic composites, Polymer Testing 26 (2007) 154–161.
[31] D. Bellett, F. Morel, A. Morel, J. Lebrun, A biaxial fatigue specimen for uniaxial loading, Strain 47 (2011) 227–240.
[33] I. Zidane, C. Zhang, D. Guines, L. Léotoing, E. Ragneau, Optimisation of biaxial tensile specimen shape from numerical investigations, Numisheet 45 (2008) 235–248.
[34] CorrelManuV, 2005. Doc. Available from: http://www.lms.polytechnique.fr/users/bornert/34_14/doc.
[35] R. Bracewell, Fast Fourier Transform and its Applications, McGraw Hill Higher Education, 1999.
[36] www.wolfram.com.